Flexural behaviour of hot-finished high strength steel square and rectangular hollow sections

J. Wang[a], S. Afshan[b,*], M. Gkantou[c], M. Theofanous[c], C. Baniotopoulos[c], L. Gardner[a]

[a]*Imperial College London, London, UK*
[b]*Brunel University London, London, UK*
[c]*University of Birmingham, Birmingham, UK*

Abstract

High strength steels, considered in the context of the structural Eurocodes, as steels with a yield strength over 460 MPa, are gaining increasing attention from structural engineers and researchers owing to their potential to enable lighter and more economic structures. This paper focuses on the bending strength of hot-finished high strength steel (HSS) square and rectangular hollow sections; the results of detailed experimental and numerical studies are presented and structural design rules for HSS cross-sections are proposed. A total of 22 in-plane bending tests, in three-point bending and four-point bending configurations, on HSS sections in grades S460 and S690 were conducted. The experimental results were replicated by means of non-linear finite element modelling. Upon validation of the finite element models, parametric studies were performed to assess the structural response of HSS sections over a wider range of cross-section slenderness, cross-section aspect ratio and moment gradient. The experimental results combined with the obtained numerical results were used to assess the suitability of the current European (EN 1993-1-1 and EN 1993-1-12) cross-section classification limits for HSS structural components. The reliability of the proposed cross-section classification limits was verified by means of the EN 1990 - Annex D method.

Keywords: Bending, Eurocode 3, Experiments, High strength steel, Hot-finished, Moment capacity, Slenderness limits, Testing.

1. Introduction

High strength steels (HSS), with yield strengths in excess of 460 MPa, are being increasingly utilised in construction, and in particular in structural applications where long and column-free spans are an important design requirement [1]. The use of high strength steels, in place of ordinary carbon steels, can enable the selection of structural elements with smaller cross-section sizes, resulting in significant material savings. This, combined with lower transportation and construction costs, bring clear advantages for high strength steel as a sustainable and economical construction material. Recent examples of structures that have made substantial use of HSS are the National Stadium in China [2] and the roof trusses in the Sony Centre in Germany [3].

---

*Corresponding author
Email address:* Sheida.Afshan@brunel.ac.uk (S. Afshan)

Previous research into the behaviour and design of HSS structures has included studies of the material characteristics described in references [4–13], residual stress measurements set-out in references [5–7, 10, 11, 14–19], global buckling behaviour of long columns explained in references [5, 8, 16, 17, 20, 21], local buckling response of stub columns and beams described in references [6, 7, 15, 22–26] and [7, 10, 15, 27, 28], respectively, as well as the behaviour of HSS members under cyclic loading [12]. It is worth noting that previous experimental studies of HSS structures were conducted on either welded or cold-formed sections, leaving the structural behaviour of hot-finished HSS sections unexplored. Therefore, as part of a wider study of the structural behaviour of hot-finished HSS square and rectangular hollow sections (SHS and RHS, respectively) the main focus of this paper is to report on an investigation of the flexural behaviour of these components. The local buckling behaviour of HSS plate elements in welded sections and cold-formed sections has been studied in references [6, 7, 15, 24, 25] and [22, 23, 26], respectively. Based mainly on the results of stub column tests, it was found that HSS outstand elements (i.e. plate elements with one longitudinal edge simply supported and the other free, e.g. the flanges of I-sections) exhibit superior local buckling performance to those of ordinary carbon steels, whilst for internal elements (i.e. plates simply supported along both longitudinal edges, e.g. the flanges of SHS/RHS), HSS and ordinary steels were found to exhibit comparable local buckling resistance [6]. In addition, the flexural behaviour of HSS cross-sections has been studied in references [7, 10, 15, 27, 28], showing that HSS beams possess lower rotation capacity compared to their ordinary steel counterparts, which can be detrimental for plastic and seismic design.

EN 1993-1-12 [29] provides additional rules that can be used in conjunction with the other parts of EN 1993 to design structures using steel grades S460 up to S700. In common with equivalent design standards for high strength steel structures [30–33], EN 1993-1-12 makes extensive reference to the design rules for ordinary carbon steel in EN 1993-1-1 [34]. In fact, while the material ductility requirements and the design of connections specific to high strength steels are set out in EN 1993-1-12 [29], the design of structural components at both cross-section level and member level is carried out in the same manner as for ordinary carbon steels. Hence, for the treatment of local buckling in HSS sections, EN 1993-1-12 [29] refers to EN 1993-1-1 [34], where cross-sections are classified into the four conventional classes based on the slenderness of the cross-section. Owing partly to the limited existing test data during the development of EN 1993-1-12 [29], the same cross-section classification limits used for ordinary carbon steel [34] are also adopted for HSS sections. The intent of this paper, therefore, is to investigate whether the current Eurocode slenderness limits are applicable to HSS hot-finished square and rectangular hollow sections in light of a larger pool of test and numerical structural performance data.

A comprehensive experimental programme on grades S460 and S690 HSS square and rectangular hollow sections was carried out at Imperial College London. The programme consisted of material tests, stub column tests, combined axial load and bending tests and in-plane bending tests on a total of eleven SHS/RHS section sizes. While this paper reports on the results of the in-plane bending tests and the associated analysis of the results, a full description of the other tests are reported in [35]. Accurate finite element models of the beam tests were also developed and, once validated, were

used to perform parametric studies, where the effect of variations of cross-section slenderness, cross-section aspect ratio, moment gradient and material grade on the structural performance of HSS hot-finished hollow SHS/RHS were investigated. Based on the combination of the obtained experimental and numerical results, the suitability of existing cross-section classification limits for HSS internal elements in compression are assessed.

2. Experimental study

2.1. Introduction and material testing

A total of 22 in-plane bending tests, in three-point bending and four-point bending configurations, were carried out to investigate the flexural response of SHS and RHS high strength steel beams. The tested specimens were of grades S460 and S690. Both materials consisted of hot-rolled base materials and were hollowed out in a piercing mill to the final shape, after which the S460 sections were normalized, whereas the S690 were quenched and tempered. The chemical compositions and the tensile material properties of the tested specimens, as provided by the mill certificates, are presented in Tables 1 and 2, respectively. Material tensile and compressive coupon tests were also performed to determine the engineering stress-strain response of the flat and corner material for each of the tested section sizes. The resulting material properties were used in the subsequent analysis of the bending test results and also in the development of the numerical models of the tested specimens. Full details of the material tests are reported in [35], while a summary of the test results is given herein in Table 3, showing tensile flat (TF), tensile corner (TC) and compressive flat (CF) coupon results. The material parameters reported in Table 3 are the Young's modulus E, the upper yield strength f_y, the ultimate tensile strength f_u, the tensile-to-yield stress ratio f_u/f_y, the strain at the ultimate tensile stress ε_u, and the plastic strain at fracture ε_f, based on elongation over the standard gauge length equal to $5.65\sqrt{A_c}$, where A_c is the cross-sectional area of the coupon. It should be noted that for each section, either two or four tensile flat coupons were tested, and the TF results displayed in Table 3 are the averaged values of the TF coupons from each section. Figures 1a and 1b show typical measured stress-strain curves for tensile flat, compressive flat and tensile corner coupons extracted from the S460 RHS $100 \times 50 \times 6.3$ and S690 RHS $50 \times 50 \times 5$ sections, respectively. From Table 3 and Figures 1a and 1b, it can be seen that both grades of material display a sharply-defined yield point, while the S690 materials generally exhibit less strain hardening and lower ductility in comparison with the S460 coupons, as measured by the tensile-to-yield ratio and the ultimate and fracture strains.

2.2. Geometric imperfection measurements

Measurements of initial geometric imperfections is important for enabling accurate modelling of the structural response of tested specimens in finite element simulations. Since lateral torsional buckling was precluded, due to the closed nature of the tested cross-sections and short length (i.e. low $\bar{\lambda}_{LT}$) of the beam specimens, only local geometric imperfections needed to be considered herein. Hence, measurements of the initial local geometric imperfection amplitudes were conducted prior to testing, following the procedures outlined in [36]. A displacement transducer

3

mounted on the head of a milling machine was moved along the central 900 mm length of each of the 1700 mm beam specimens. A total of three runs, one in the middle and two close to the edges of each of the faces of the sections, were recorded. The obtained results were used to determine the maximum deviations from a flat datum for each of the four faces of each section, and the maximum of those values are reported in Table 4 and denoted ω_0. The average measured geometric dimensions of the beam specimen are also provided in Table 4, where L is the beam length, h is the section depth, b is the section width, t is the thickness and r_i is the average internal corner radius.

2.3. Residual stress measurements

Residual stresses are the self-equilibrating internal stresses that exist within a structural member in its unloaded state. Residual stress measurements on a sample of the S690 SHS $90 \times 90 \times 5.6$ were made as part of the present study. Using the sectioning method, the SHS $90 \times 90 \times 5.6$ specimen was divided into strips, and a Whittemore gauge was used to measure the strains on the outer and inner surfaces of the strips of material prior to and after sectioning. Since no curving of the strips was observed, it was concluded that no bending residual stresses existed, and the measured residual strains were associated with axial membrane residual stresses only. The residual stresses were computed by multiplying the average of the inner and outer relieved strains (which were consistently very close values) by the measured Young's moduli from the tensile and compressive coupon tests (matching the direction of the strains), and their distribution around the cross-section is shown in Figure 2. The maximum measured longitudinal membrane residual stresses were $0.055f_y$ in tension and $0.031f_y$ in compression.

2.4. Beam tests

Three-point bending tests and four-point bending tests were conducted to establish a relationship between cross-section slenderness and the moment capacity and rotation capacity of HSS hollow sections. Adopting these two bending configurations allowed comparisons of the basic flexural response characteristics of HSS beams under constant moment (four-point bending tests) and a moment gradient (three-point bending tests). All specimens had a total length of 1700 mm, with equal overhangs at each end of 50 mm beyond the centrelines of the supports (i.e. the span of the beams were 1600 mm). Simple support conditions were achieved by means of steel rollers located between two steel plates as shown in Figures 3 and 4, which allowed rotation about the axis of bending as well as axial displacements at the two ends of the beams. The tested beams were loaded symmetrically, in an Instron 2000 kN hydraulic testing machine, at mid-span and at third-points for the three-point bending and four-point bending arrangements, respectively, as shown in Figures 3 and 4. In all cases bending was about the cross-section major axis.

Wooden blocks, with dimensions tightly matching those of the tested beam sections, were inserted within the tubes at the loading points and at the supports to prevent web crippling under the localised point loading. Linear electrical resistance strain gauges were affixed to the top and bottom flanges of the beam sections at mid-span and at a distance of 60 mm from the mid-span for the four-point bending and for the three-point bending tests, respectively, to measure

4

the extreme tensile and compressive strains. Linear variable differential transformers (LVDT) located at mid-span, for the three-point bending tests, and at both mid-span and at the loading points, for the four-point bending tests, were used to measure the vertical deflections. Two inclinometers were positioned at the support locations to measure end rotations in the three-point bending tests. The test set-up was displacement controlled at a cross-head displacement rate of 4 mm/min for the specimens loaded in three-point bending, apart from the S460 SHS $50 \times 50 \times 4$ specimen where a lower rate of 2 mm/min was used, and 3 mm/min for all four-point bending tests. Test data including load, strain, displacement and end rotation were all recorded using the data acquisition equipment DATASCAN and logged at 1 sec intervals using the DSLOG computer package.

The key results from the tests, including the ultimate test bending moment M_{max} and the cross-section rotation capacity R are reported in Tables 5 and 6 for three-point bending and four-point bending, respectively. The calculated cross-section elastic moment M_{el} and plastic moment M_{pl} capacities, given as the product of the measured material yield strength f_y, from Table 3, and the respective section modulus (elastic section modulus W_{el} or plastic section modulus W_{pl}) based on the measured geometry, together with the local slenderness of the compression flange $c/t\varepsilon$ (as defined in Section 3.2), are also reported in Tables 5 and 6. Figures 5a and 5b show the non-dimensional mid-span moment-rotation and moment-curvature responses from the three-point and four-point bending tests, respectively, for the grade S460 beams, while the equivalent response characteristics are shown in Figures 6a and 6b for the grade S690 beams, θ is the mid-span rotation, taken as the sum of the two end rotations from the inclinometer measurements, θ_{pl} is the elastic component of the rotation at M_{pl}, κ is the curvature and κ_{pl} is the elastic curvature corresponding to M_{pl}. Curvature κ in the constant moment region, of length L_2, of the four-point bending tests was determined using the measurements from the LVDTs and assuming that the deformed shape of the central span represents a segment of a circular arc (of radius r) [37], leading to the expression in Equation 1, where D_M is the vertical displacement at mid-span and D_L is the average vertical displacement at the two loading points. Based on the recorded moment-rotation and moment-curvature responses, the rotation capacity R was determined from Equations 2 and 3 for the three-point bending and four-point bending cases, respectively, where κ_u (θ_u) is the curvature (rotation) at which the moment-curvature (moment-rotation) curve falls below M_{pl} on the descending branch, and κ_{pl} (θ_{pl}) is the elastic curvature (rotation) corresponding to M_{pl} on the ascending branch, as shown in Figure 7. The curvatures or rotations at ultimate moment are denoted κ_{max} and θ_{max}, respectively. Owing to the limited vertical displacement capacity of the test rig, some tests had to be discontinued before the full moment-rotation/curvature profiles were recorded. In cases where the ultimate moment capacity was not reached, the maximum recorded moment and rotation/curvature values are reported. In cases where the tests were stopped before the bending moment fell below M_{pl}, the maximum recorded rotation/curvatures are used to determine the rotation capacity R. These cases are highlighted in Tables 5 and 6. All test specimens, apart from those which did not reach their ultimate moment capacity, failed by yielding and local buckling of the compression flange and the compressive part of the web, as illustrated in Figures 8 and 9. The more slender sections exhibited greater susceptibility to local buckling and therefore lower normalised moment capacity and rotation capacity (ductility).

$$\kappa = \frac{1}{r} = \frac{8(D_M - D_L)}{4(D_M - D_L)^2 + L_2^2} \tag{1}$$

$$R = \frac{\theta_u}{\theta_{pl}} - 1 \tag{2}$$

$$R = \frac{\kappa_u}{\kappa_{pl}} - 1 \tag{3}$$

The difference in the flexural response of beams under four-point bending and three-point bending brought about by the different bending moment distributions are discussed in [38, 39], and can also be seen from the results of the high strength steel beam tests presented herein. Higher bending moment resistances are generally observed in three-point bending specimens relative to their four-point bending counterparts. This may be seen in the present results for specimens S460 SHS $90 \times 90 \times 3.6$, S690 SHS $100 \times 100 \times 5.6$ and S690 SHS $90 \times 90 \times 5.6$, which reached their ultimate moment capacities under both loading conditions, allowing such comparisons to be made. The higher bending moment capacities achieved under a moment gradient (i.e. three-point-bending) are attributed to the delay in local buckling due to the restraining effects from the material immediately adjacent to the plastic hinge, which is at a lower stress level. This restraining effect is not present in the constant moment region of a beam under four-point bending.

3. Numerical modelling

A numerical modelling study was carried out in parallel with the experimental programme. The main aim of this investigation was to develop validated numerical models, through accurate replication of the test results presented in Section 2, to perform parametric studies and to examine further the influence of key parameters on the flexural response of HSS tubular beams. In this section, the key characteristics of the finite element models and details of the parametric studies are presented, and the obtained results are discussed.

3.1. Validation of FE models

The general purpose finite element analysis package ABAQUS [40] was employed throughout this study. Shell elements were adopted to discretise the high strength steel beams as is commonplace for the modelling of thin-walled metallic sections [41, 42]. The finite element type S4R, a four-noded, doubly curved general-purpose shell element with reduced integration and finite membrane strains, selected from the ABAQUS [40] element library, was employed for all models. A mesh convergence study was carried out to establish a sufficiently refined mesh size which provides accurate results with practical computational times. An average element size equal to the thickness of the section was found to be suitable, and was adopted herein for the flat parts of the sections. Three elements were employed for the

corner regions. The measured geometric and material properties, obtained from the experimental investigation, were incorporated into the finite element models to replicate the corresponding test behaviour. The boundary conditions were carefully selected to simulate the experimental set-up. The vertical and lateral displacements at the bottom flange were restrained at the ends of the beams, while longitudinal displacement was prevented at the mid-span of the beam. In both the three-point bending and four-point bending models, the point loads were applied to the lower part of the web at the web-corner junction in order to prevent web crippling under concentrated loading. The symmetry of the test configuration with respect to geometry, boundary conditions, loading and the observed failure mode of the beam specimens was exploited in the numerical models by modelling only half the cross-section of each specimen. This was achieved by employing suitable symmetry boundary conditions along the assumed axis of symmetry. Also, for modelling convenience, the cross-sections at the supports were constrained through kinematic coupling in order to remain undeformed.

The measured material stress-strain curves were utilised in the development of the finite element models. The material behaviour was modelled as elastic-plastic with a Von Mises yield criterion and isotropic hardening. The material properties from the flat tensile coupons were adopted, as no significant differences in the stress-strain behaviour were observed for the corner regions or between the tensile and compressive properties. ABAQUS requires the input of the material stress-strain curves in the form of a multi-linear true stress-strain response. True stress σ_true and true plastic strain $\varepsilon_\text{true}^\text{pl}$ were obtained from the engineering stress-strain data as given by Equations 4 and 5, respectively, where σ_nom is the engineering stress, ε_nom is the engineering strain and E is the Young's modulus.

$$\sigma_\text{true} = \sigma_\text{nom}(1 + \varepsilon_\text{nom}) \tag{4}$$

$$\varepsilon_\text{true}^\text{pl} = \ln(1 + \varepsilon_\text{nom}) - \frac{\sigma_\text{nom}}{\text{E}} \tag{5}$$

All structural members contain geometric imperfections, which are defined as deviations from the ideal geometry. The behaviour of structural members can be significantly influenced by the magnitude and nature of any initial geometric imperfections, and these therefore need to be accurately accounted for in numerical simulations. In line with previous studies [41–43], local geometric imperfections were incorporated into the models in the form of the lowest elastic buckling mode shape, obtained from a linear eigenvalue buckling analysis, with suitable imperfection amplitudes. Five values of local geometric imperfection amplitudes were examined: $t/10$, $t/50$ and $t/100$, the maximum measured imperfections ω_0, as given in Table 4, and a value calculated from the predictive model of Dawson and Walker [44], as modified by Gardner and Nethercot [43], defined by Equation 6.

$$\omega_0 = \beta(\text{f}_\text{y}/\text{f}_\text{cr})^{0.5}\text{t} \tag{6}$$

where f_y is the material yield strength, f_cr is the elastic critical buckling stress of the most slender constituent plate element in the section and t is the plate thickness. In the absence of a comprehensive pool of measured local

imperfection data to calibrate Equation 6 for high strength steels, a value of 0.028 was adopted for the β parameter, as recommended for ordinary carbon steel hot-rolled rectangular hollow sections in [45]. Owing to their very low magnitudes, residual stresses (see Section 2.3) were not explicitly introduced into the FE models.

Geometrically and materially nonlinear FE models of the tested beam specimens, developed based on the above described modelling assumptions, were solved using the modified Riks method [40], which is a variation of the classic arc length method [40, 46], allowing the post-ultimate behaviour to be traced. Validation of the models was based on the comparison of the obtained numerical results with the relevant test data. To this end, the FE ultimate moment $M_{max,FE}$, the FE rotation at ultimate moment $\theta_{max,FE}$ for the three-point bending tests and the FE curvature at ultimate moment $\kappa_{max,FE}$ for the four-point bending tests were compared with their respective experimental values, $M_{max,exp}$, $\theta_{max,exp}$ and $\kappa_{max,exp}$, respectively, and are reported in Tables 7 and 8. The above results are reported for all the considered local imperfection amplitudes. As anticipated, the variation of the imperfection amplitude has only a minor influence on the ultimate moment capacity M_{max} of the beams, while the corresponding rotation θ_{max} or curvature κ_{max} at ultimate moment was shown be more sensitive. Overall, the local imperfection amplitude of $t/50$ was found to provide the closest agreement between the numerical and experimental results for both the three-point bending and four-point bending configurations. Typical comparisons of moment-rotation and moment-curvature responses from the tests and FE models are shown in Figures 10 and 11, where accurate replication of the initial stiffness, the ultimate moment capacity and general form of the load-deformation histories were achieved. Typical test and FE failure modes for the three-point bending and four-point bending configurations are depicted in Figure 12, and may be seen to match closely.

3.2. Parametric studies

Having validated the numerical models against the experimental results, a series of parametric studies were performed, focusing on variations in the cross-section slenderness, cross-section aspect ratio, moment gradient and material strain hardening characteristics. A piecewise linear material stress-strain model based on the average results of the flat tensile coupon tests was adopted. Initial local geometrical imperfections took the form of the lowest elastic local eigenmode with an amplitude equal to $t/50$. To assess the effect of strain hardening on the flexural behaviour of hot-finished high strength steel SHS and RHS, two steel grades, namely S460 and S690 were considered. Three cross-section aspect ratios $h/b = 1.00$, 2.00 and 2.44 were used to examine the effect of plate element interaction on the bending response of HSS sections. The effect of cross-section slenderness was investigated by varying the cross-section thickness, while maintaining the cross-section outer dimensions. A total of nine different section thicknesses were considered, providing a range of $c/t\varepsilon$ ratios from 10 to 90, where c is the compressed flat width, t is the plate thickness and $\varepsilon = \sqrt{235/f_y}$. Three test configurations including three-point bending with a span-to-depth ratio $L/h = 10$, three-point bending with $L/h = 20$ and 4-point bending with $L/h = 20$ were also investigated. A total of 216 parametric FE simulations were performed, and the obtained results are discussed in detail in the following section.

It is worth noting that, based on the EN 1993-1-5 [47] plate slenderness definition $\bar{\lambda}_p = (f_y/f_{cr})^{0.5}$ and making due allowance for the type of stress distribution through the k_σ coefficient of the flange and web elements, $h/b = 2.44$ is the limiting aspect ratio at which the flange element in compression (with $k_\sigma = 4.0$) and web element in bending (with $k_\sigma = 23.9$) have equal plate slenderness values. Hence $h/b = 2.44$ represents the most unfavourable aspect ratio for box sections in bending in the sense that the section comprises equally slender flange and web elements, and therefore no benefit from the effects of plate element interaction on the local buckling response of the cross-section arises.

4. Analysis of results and design recommendations

In this section, the results of the parametric studies are presented and discussed. This is followed by an assessment of the existing cross-section classification limits provided in Eurocode 3 [29, 34] for internal elements in compression against the generated test and FE data to evaluate their applicability to high strength steel hollow sections. On the basis of the comparisons, suitable design recommendations are then presented. Note that throughout this section, measured geometric and material properties, based on the average flat coupon tests results, are adopted in all comparisons, and all partial safety factors are set to unity.

4.1. Influence of material strain hardening

The relationship between M_{max}/M_{pl}, where M_{max} is the test or FE ultimate moment and M_{pl} is the cross-section plastic moment capacity, and the EN 1993-1-1 slenderness parameter $c/t\varepsilon$ of the most slender constituent element in the cross-section is plotted in Figure 13a for the S460 and S690 steel beams under the same moment gradient. In determining the most slender element, account of the stress distribution and element support conditions has been made through the buckling factor k_σ, as defined in EN 1993-1-5. Similarly, Figure 13b shows the variation of the test and FE cross-section rotation capacity R, obtained from Equations 2 and 3, with the slenderness parameter $c/t\varepsilon$ for the S460 and S690 steel beams under the same moment gradient. In both Figures 13a and 13b, the results are presented for the three different investigated cross-section aspect ratios. From the figures, it is evident that the stocky S460 steel beams are capable of reaching higher normalised bending moment capacities, of up to 50% in excess of their plastic moment resistance M_{pl}, compared with the stocky grade S690 beams. This is expected owing to the higher strain hardening level exhibited by the S460 grade. Higher rotation capacities were also achieved by the grade S460 beams compared with the grade S690 beams. This may be anticipated since higher levels of strain hardening, reflected by the higher material f_u/f_y ratio, correspond to higher average tangent stiffnesses in the inelastic range, which delay the onset of local buckling, while after the onset of local buckling, a higher degree of strain hardening enables a greater relative contribution from the post-buckling membrane stresses. Further studies on the influence of strain hardening on the rotation capacity of steel beams have been reported by [27, 48]. As expected, in the more slender range, where failure is triggered by cross-section local buckling at strains within or below the yield plateau, the influence of material grade on the normalised response is minimal.

4.2. Influence of cross-section aspect ratio

In Figure 13a, the effect of the cross-section aspect ratio on the normalised bending moment capacity of HSS sections can be observed by considering the results of the more slender cross-sections, which are largely independent of material grade since failure is predominantly in the elastic range. The results show that for a given moment gradient (determined from the test configuration) and cross-section slenderness, the normalised flexural performance improves with decreasing aspect ratio. This is expected owing to the increase in the beneficial effects of plate element interaction on the local buckling performance of the compression flange, which is the critical element in the cross-section when $h/b < 2.44$, with decreasing aspect ratio. In the stocky range, where the failure of the specimens is mainly governed by material yielding, the effect of aspect ratio on the cross-section ultimate moment capacity is significantly reduced, though a notable influence on the rotation capacity remains, as shown in Figure 13b.

4.3. Influence of moment gradient

To examine the effect of moment gradient on the normalised flexural response of hot-finished HSS hollow sections, the ultimate to plastic moment ratio M_{max}/M_{pl} and rotation capacity R from both the test and parametric FE results, with a fixed aspect ratio of $h/b = 2$, are plotted against the $c/t\varepsilon$ slenderness parameter in Figures 14a and 14b, respectively. Four-point bending results are not considered in Fig. 14b, since the calculation of the rotation capacity for four-point bending tests is based on curvatures, rather than rotations and the results are therefore not directly comparable. The moment gradient is seen to have a fairly minimal influence on the normalised moment capacity of high strength steel beams (see Figure 14a), but a more pronounced effect on the cross-section rotation capacity R of the beam specimens as shown in in Figure 14b, where beams with $L/h = 10$ display higher rotation capacity than the corresponding beams with $L/h = 20$. Similar conclusions have been reached by other researchers [27, 39, 48].

4.4. Assessment of Eurocode slenderness limits for internal elements in compression

In the European structural steel design standards, EN 1993-1-1 [34] and EN 1993-1-12 [29], the concept of cross-section classification is used for the treatment of local buckling. The classification of the plate elements within the cross-sections is based on their width-to-thickness ratio (c/t), the material properties, the edge support conditions and the form of the applied stress field. The overall cross-section classification is assumed to relate to its most slender constituent element. EN 1993-1-12 [29] adopts the same classification limits for high strength steel as are set out for ordinary strength steel in EN 1993-1-1 [34], but with the restriction that plastic design is not permitted for high strength steel structures. This means that for high strength steel, there is in fact no distinction between Class 1 and Class 2 cross-sections. In this section, the current slenderness limits for internal elements in compression are assessed against the assembled experimental and numerical data on high strength steel hot-finished structural hollow sections. In addition, the recently proposed modifications to the Eurocode 3 slenderness limits [49], which are approximately in line with the recently revised limits for stainless steel [50], are also considered.

4.4.1. Class 1 slenderness limit

Although plastic design is not currently permitted in EN 1993-1-12, assessment of the Class 1 limit is nonetheless made based on a required rotation capacity R of at least 3, which is the value used in the development of EN 1993-1-1 for the plastic design of steel structures up to grade S460 [34]. In Figure 15, the rotation capacity R from both the test and FE models is plotted against the local slenderness $c/t\varepsilon$ of the flange. Test data on steel beams with nominal yield strengths between 350 N/mm^2 and 450 N/mm^2 collected from the literature [45, 51, 52] are also presented in Figure 15 for comparison purposes. The Class 1 slenderness limit specified in EN 1993-1-1 [34] and that proposed in [49] along with the rotation capacity limit of R = 3 [53] are also shown in Figure 15. While the EN 1993-1-1 Class 1 limit of 33 appears inappropriate for HSS hollow sections, its use for ordinary carbon steel is also questionable. The lower proposed limit of 28 provides safer predictions for both ordinary carbon steel and high strength steel, and given the high scatter associated with rotation capacity data and the historical use of the more relaxed limit of 33, the proposed limit [49] of $c/t\varepsilon = 28$ is deemed appropriate. Further research is clearly needed into the possibility of allowing the use of plastic design for high strength steel structures.

4.4.2. Class 2 slenderness limit

The Class 2 slenderness limits specified in EN 1993-1-1 and proposed in [49], together with the test and FE results from this study of high strength steel and the test data from [45, 51, 52] on lower grades of steel, are shown in Figure 16, where the ultimate moment capacity M_{max} has been normalised by the plastic moment capacity M_{pl}, and plotted against the $c/t\varepsilon$ ratio of the flange. From Figure 16, the current Class 2 limit of 38 appears slightly high, particularly for the FE results on the cross-sections with higher aspect ratios, whereas the lower proposed limit of 34 generally provides a lower bound to the test data and a better match to the FE results on the cross-sections with high aspect ratios. In general, there appears to be no significant differences in the trends shown by the beams of the lower and higher strength materials.

4.4.3. Class 3 slenderness limit

In Figure 17, the ultimate moment capacity M_{max} obtained from the test and numerical results is normalised by the elastic moment capacity M_{el} and plotted against the $c/t\varepsilon$ ratio of the compression flange, allowing the assessment of the Class 3 limits. The results show that the current EN 1993-1-1 slenderness limit of 42 for fully effective sections is also applicable to high strength steel square and rectangular hollow sections, but is rather on the safe side. Similar conservatism is also observed for the bending test results on the lower grade materials [45, 51, 52]. However, a stricter Class 3 limit of 38 was proposed in [49] for the case of ordinary carbon steel sections, based on the results of stub column tests; this limit was also shown to be suitable for high strength steels in [35]. Adoption of the proposed Class 3 limit of 38 is therefore supported in this study. The results also support the inclusion of a linear transition [49] from M_{pl} to M_{el} for Class 3 sections, rather than the current step change in bending moment capacity at the Class 2 to 3 boundary.

4.5. Reliability analysis

Statistical analyses in accordance with Annex D of EN 1990 [54] were performed to assess the reliability of the proposed Class 2 and Class 3 slenderness limits for high strength steel internal elements in compression. Owing to the high scatter associated with measured rotation capacity data, a reliability assessment has not been performed for the Class 1 limit; this is consistent with previous studies [53]. The test data reported in Section 2 and the numerical results from the parametric studies performed in Section 3 are used in the statistical analyses.

Based on a total of 1600 tensile coupon test results collected from steel producers, the mean to nominal yield strength ratio $f_{y,mean}/f_{y,nom}$ (i.e. the over-strength) and coefficient of variation of the yield strength V_{f_y} were found to be 1.12 and 0.0499 and 1.15 and 0.0605 for S460 and S690 high strength steel, respectively. Representative mean values of $f_{y,mean}/f_{y,nom}$ and V_{f_y} equal to 1.135 and 0.055 were adopted for both high strength steel grades in the analyses carried out herein. Similar values of $f_{y,mean}/f_{y,nom} = 1.16$ and $V_{f_y} = 0.05$ were adopted by Byfield and Nethercot [55] for lower grades of steel. The coefficient of variation of the geometric properties was taken as 0.02 [55]. To add artificial variability to the numerical results, an additional variability term namely V_{FE}, was also incorporated in the reliability analysis. The coefficient of variation of the numerical model V_{FE} was determined by considering the deviation between the experimental and numerical results, as used in similar studies in [56, 57], giving a value of 0.035.

For the purpose of the reliability analyses performed herein, the design resistance equations for a cross-section in bending set out in *Clause 6.2.5* of EN 1993-1-1, as given by Equations 7-8, were expressed in a modified form as presented in Equations 9 and 10, where γ_{M0} is the partial safety factor and the $\alpha_{c,Rd}$ coefficients provide a linear relationship between the predicted moment capacity $M_{c,Rd}$ and the local slenderness parameter $c/t\varepsilon$. The relationships between $\alpha_{c,Rd}$ and $c/t\varepsilon$ were established by fitting linear regression lines through the relevant experimental and numerical results, as shown in Figures 18 and 19, for the assessment of the Class 2 and Class 3 slenderness limits, respectively. The EN 1990 Annex D method was applied to the theoretical resistance functions r_t, presented in Equations 9 and 10, to determine their corresponding design resistance functions r_d, obtained from Equation 11. In Equation 11, b is the mean value correction factor, r_t is the theoretical resistance function evaluated for the mean (measured) values of the basic variables, $k_{d,n}$ is the design fractile factor for n data points and $k_{d,\infty}$ is the design fractile factor for n tending to infinity. The remaining parameters $(\alpha_{rt}, \alpha_\delta, Q_{rt}, Q_\delta, Q)$ are the reliability analysis parameters as defined in Annex D of EN 1990 [54]. To allow for the effect of the material over-strength (i.e. f_{mean}/f_{nom}), the design resistance equations were multiplied by this ratio and plotted in Figures 18 and 19. The required partial safety factor for the Class 2 and Class 3 slenderness limits were therefore defined as the ratio of the nominal resistance, from the EC3 resistance model, to the design resistance $(r_d \times f_{y,mean}/f_{y,nom})$, as illustrated in Figures 18 and 19. As shown in Figure 19, the $(r_d \times f_{y,mean}/f_{y,nom})$ line passes though the nominal resistance line corresponding to unity on the vertical axis (i.e. $M = M_{el}$) almost exactly at the Class 3 slenderness limit of 38 , resulting in a γ_{M0} value of 1.0. For the Class 2 limit, see Figure 18, the $(r_d \times f_{y,mean}/f_{y,nom})$ line lies below the nominal resistance line (i.e. $M = M_{pl}$),

and a required value of γ_{M0} of 1.18 is determined.

$$M_{c,Rd} = \frac{W_{pl}f_y}{\gamma_{M0}} \qquad \text{for Class 1 and 2 sections} \qquad (7)$$

$$M_{c,Rd} = \frac{W_{el}f_y}{\gamma_{M0}} \qquad \text{for Class 3 sections} \qquad (8)$$

$$M_{c,Rd} = \alpha_{c,Rd}W_{pl}f_y \qquad \text{for Class 1 and 2 sections} \qquad (9)$$

$$M_{c,Rd} = \alpha_{c,Rd}W_{el}f_y \qquad \text{for Class 3 sections} \qquad (10)$$

$$r_d = br_t\exp(-k_{d,\infty}\alpha_{rt}Q_{rt} - k_{d,n}\alpha_\delta Q_\delta - 0.5Q^2) \qquad (11)$$

Table 9 provides a summary of the key statistical parameters obtained, where $k_{d,n}$ is the design (ultimate limit state) fractile factor for n tests, where n is the population of test and FE data under consideration; b is the average ratio of experimental and FE to model resistance (Equations 9 and 10) based on a least squares fit to the data; V_δ is the coefficient of variation of the test and FE results relative to the resistance model; and V_r is the combined coefficient of variation incorporating the resistance model, the numerical model and the basic variable uncertainties. Note that the b values reported in Table 9 were derived based on the resistance models of Equations 9 and 10. The results of the reliability analysis based on the existing EN 1993-1-1 Class 2 and Class 3 limits are also reported in Table 9 for comparison purposes. The results show that the current and proposed Class 3 limits are clearly acceptable, with required partial factors γ_{M0} very close to unity, which is the recommended value in EN 1993-1-1. For the Class 2 limit, the required partial factors γ_{M0} implied by the EN 1990 analyses are close to 1.20, indicating that the required safety level is not achieved. However, given the similarity of the high strength steel results to those of the lower steel grades, and the historic use of the Class 2 slenderness limit of 38, the proposed stricter limit of 34 is deemed acceptable for both normal and high strength steels.

5. Conclusions

An experimental programme comprising a total of 22 in-plane bending tests, in three-point bending and four-point bending configurations, on hot-finished high strength steel structural hollow sections was described in this paper. Numerical models, validated against the obtained test data, were developed and used to further assess the influence of key parameters, including material strain hardening, cross-section aspect ratio and moment gradient, on the structural response of HSS hollow sections. The experimental and numerical results generated were then used to assess the applicability of the Eurocode 3 [29, 34] cross-section classification limits to high strength steel internal elements in compression. The recently proposed amendments to the Eurocode 3 cross-section slenderness limits for ordinary

carbon steel sections provided in [49] were also considered. It was shown that based on a rotation capacity requirement of R = 3, a Class 1 slenderness limit of 28, as proposed in [49] is acceptable for high strength steel internal elements in compression. Similarly, the stricter Class 2 limit of 34 proposed in [49] was shown to be more suitable than the current codified limit of 38 for high strength steel internal elements in compression. Finally, while the current codified Class 3 limit of 42 was found to be applicable to high strength steel internal elements in compression on the basis of the presented bending tests, the results of stub column tests on high strength steel hollow sections in [35] revealed that a lower value of 38 [49] is more appropriate, and is therefore recommended herein. Overall, the behavioural trends exhibited by the examined high strength steel beams follow those observed for lower grades of material, and the results presented herein support the adoption of the revised slenderness limits proposed in [49] in Eurocode 3 for both normal and high strength steels.

6. Acknowledgements

7. References

[1] Samuelsson A. and Schröter F. Chapter 5.1 - Production processes, mechanical and chemical properties, fabrication properties. In *Use and application of high-performance steels for steel structures*. International Association for Bridge and Structural Engineering (IABSE), 2005.

[2] Fan Z., Liu X. M., Fan X. W., Hu C. Y., Hu T. B., Wu X. M., and Yu Y. Q. Design and research of large-span steel structure for the national stadium. *Journal of Building Structures*, 28:1–16, 2007.

[3] Höglund T., Collin P., Müller C., Schröter F., and Miazzon A. Chapter 5.5 - Examples and applications. In *Use and application of high-performance steels for steel structures*. International Association for Bridge and Structural Engineering (IABSE), 2005.

[4] Ban H. Y., Shi G., Shi Y. J., and Wang Y. Q. Overall buckling behavior of 460 MPa high strength steel columns: Experimental investigation and design method. *Journal of Constructional Steel Research*, 74:140–150, 2012.

[5] Ban H. Y., Shi G., Shi Y. J., and Bradford M. A. Experimental investigation of the overall buckling behaviour of 960 MPa high strength steel columns. *Journal of Constructional Steel Research*, 88:256–266, 2013.

[6] Rasmussen K. J. R. and Hancock G. J. Plate slenderness limits for high strength steel sections. *Journal of Constructional Steel Research*, 23:73–96, 1992.

[7] Beg D. and Hladnik L. Slenderness limit of Class 3 I cross-sections made of high strength steel. *Journal of Constructional Steel Research*, 38(3):201–217, 1996.

[8] Shi G., Ban H. Y., and Bijlaard F. S. K. Tests and numerical study of ultra-high strength steel columns with end restraints. *Journal of Constructional Steel Research*, 70:236–247, 2012.

[9] Kim D. K., Lee C. H., Han K. H., Kim J. H., Lee S. E., and Sim H. B. Strength and residual stress evaluation of stub columns fabricated from 800 MPa high-strength steel. *Journal of Constructional Steel Research*, 102:111–120, 2014.

[10] Lee C. H., Han K. H., Uang C. M., Kim D. K., Park C. H., and Kim J. H. Flexural strength and rotation capacity of I-shaped beams fabricated from 800-MPa steel. *Journal of Structural Enigneering, ASCE*, 139(6):1043–1058, 2013.

[11] Nishino F., Ueda Y., and Tall L. Experimental investigation of the buckling plates with residual stress. Technical report, Firtz Enineering Laborarory Report No. 290.3, Lehigh University, Bethlehem, Pennsylvania, USA, 1966.

[12] Wang Y. B., Li G. Q., Cui W., Chen S. W., and Sun F. F. Experimental investigation and modeling of cyclic behavior of high strength steel. *Journal of Constructional Steel Research*, 104:37–48, 2015.

[13] Langenberg P., Niessen T., and Dahl W. Bruch- und Verformungsverhalten von hochfesten Stäehlen mit Streckgrenzen von 690 bis 890 MPA. *Stahlbau*, 69:291–283, 2000. In German.

[14] Ban H. Y., Shi G., Shi Y. J., and Wang Y. Q. Residual stress of 460 MPa high strength steel welded box section: Experimental investigation and modeling. *Thin-Walled Structures*, 64:73–82, 2013.

[15] Usami T. and Fukumoto Y. Welded box compression members. *Journal of Structural Engineering, ASCE*, 110(10):2457–2470, 1984.

[16] Wang Y. B., Li G. Q., Chen S. W., and Sun F. F. Experimental and numerical study on the behavior of axially compressed high strength steel columns with h-section. *Engineering Structures*, 43:149–159, 2012.

[17] Wang Y. B., Li G. Q., Chen S. W., and Sun F. F. Experimental and numerical study on the behavior of axially compressed high strength steel box-columns. *Engineering Structures*, 58:79–91, 2014.

[18] Uy B. Strength of short concrete filled high strength steel box columns. *Journal of Constructional Steel Research*, 57:113–122, 2001.

[19] Shi G., Shi Y. J., and Ban H. Y. *Gao qiang du gang cai gang jie gou (Steel structures made of high strength steel)*. China Architecture and Building Press, 2014. In Chinese.

[20] Rasmussen K. J. R. and Hancock G. J. Test of high strength steel columns. *Journal of Constructional Steel Research*, 34:27–52, 1995.

[21] Yang D. M., Hancock G. J., and Rasmussen K. J. R. Compression tests of cold-reduced high strength steel sections. II:long columns. *Engineering Structures*, 130(11):1782–1789, 2004.

[22] Yang D. M. and Hancock G. J. Numerical simulation of high-strength steel box-shaped columns failing in local and overall buckling modes. *Engineering Structures*, 132(4):541–549, 2006.

[23] Yang D. M. and Hancock G. J. Compression tests of cold-reduced high strength steel sections. I:stub columns. *Engineering Structures*, 130(11):1772–1781, 2004.

[24] Yoo J. H., Kim J. W., Yang J. G., Kang J. W., and Lee M. J. Local buckling in the stub columns fabricated with HSA800 of high performance steel. *International Journal of Steel Structures*, 13(3):445–458, 2013.

[25] Shi G., Zhou W. J., Bai Y., and Lin C. C. Local buckling of 460 MPa high strength steel welded section stub columns under axial compression. *Journal of Constructional Steel Research*, 100:60–70, 2014.

[26] Gao L., Sun H. C., Jin F. N., and Fan H. L. Load-carrying capacity of high-strength steel box-sections I:Stub columns. *Journal of Constructional Steel Research*, 65:918–924, 2009.

[27] Ricles J. M., Sause R., and Green P. S. High-strength steel: implications of material and geometric characteristics on inelastic flexural behavior. *Engineering Structures*, 20(4-6):323–335, 1998.

[28] McDermott J. F. Plastic bending of A514 steel beams. *Journal of the Structural Division, ASCE*, 95(9):1851–1871, 1969.

[29] EN 1993-1-12. *Eurocode 3: Design of steel structures. Part 1-12: Additional rules for the extension of EN 1993 up to steel grades S700*. European Committee for Standardization (CEN), 2006.

[30] ANSI/AISC 360-10. *Specification for structural steel buildings*. American Institute of Steel Construction, 2005.

[31] ANSI/AISC 341-05. *Seismic provisions for structural steel buildings*. American Institute of Steel Construction, 2005.

[32] GB 50017-2003. *Code for design of steel structures*. Beijing: Standards Press of China, 2003. In chinese.

[33] AS 4100-1998. *Steel structures*. Standard Association of Australia, 1998.

[34] EN 1993-1-1. *Eurocode 3: Design of steel structures. Part 1-1: General rules and rules for buildings*. European Committee for Standardization (CEN), 2005.

[35] Wang J., Schillo N., Afshan S., Theofanous M., Feldmann M., and Gardner L. Material properties and local buckling behaviour of high strength steel square and rectangular hollow sections. *Journal of Constructional Steel Research*, Submitted.

[36] Schafer B. W. and Pekz T. Computational modeling of cold-formed steel: characterizing geometric imperfections and residual stresses. *Journal of Constructional Steel Research*, 47:193–210, 1998.

[37] Rasmussen K. J. R. and Hancock G. J. Design of cold-formed stainless steel tubular members. II:Beams. *Journal of Structural Engineering, ASCE*, 119(8):2368–2386, 1993.

[38] Chan T. M. and Gardner L. Bending strength of hot-rolled elliptical hollow sections. *Journal of Constructional Steel Research*, 64:971–986, 2008.

[39] Lay M. G. and Galambos T. V. Inelastic beams under moment gradient. *Journal of the Structural Division, ASCE*, 93(1):381–399, 1967.

[40] Hibbitt, Karlsson, and Sorensen Inc. ABAQUS. *ABAQUS/Standard user's manual volume IIII and ABAQUS CAE manual.Version 6.10*. USA: Pawtucket, 2010.

[41] Zhou F., Tong L. W., and Chen Y. Y. Experimental and numerical investigations of high strength steel welded H-section columns. *International Journal of Steel Structures*, 13(2):209–218, 2013.

[42] Theofanous M. and Gardner L. Experimental and numerical studies of lean duplex stainless steel beams. *Journal of Constructional Steel Research*, 66:816–825, 2010.

[43] Gardner L. and Nethercot D. A. Numerical modeling of stainless steel structural components - A consistent approach. *Journal of Structural Engineering, ASCE*, 130(10):1586–1601, 2004.

[44] Dawson R. G. and Walker A. C. Post-buckling of geometrically imperfect plates. *Journal of the Structural Division, ASCE*, 98(1):75–94, 1972.

[45] Gardner L., Saari N., and Wang F. C. Comparative experimental study of hot-rolled and cold-formed rectangular hollow sections. *Thin-Walled Structures*, 48(7):495–507, 2010.

[46] Riks E. An incremental approach to the solution of snapping and buckling problems. *International Journal of Solids and Structures*, 15(7):529–551, 1978.

[47] EN 1993-1-5. *Eurocode 3: Design of steel structures. Part 1-5: Plated structural elements*. European Committee for Standardization (CEN), 2006.

[48] Kuhlmann U. Definition of flange slenderness limits on the basis of rotation capacity values. *Journal of Constructional Steel Research*, 14:21–40, 1989.

[49] Taras A., Greiner R., and Unterweger H. Proposal for amended rules for member buckling and semi-compact cross-section design. Technical report, Consolidated version of documents of the same title submitted to the SC3 Evolution Group 1993-1-1, Paris, 2013.

[50] Gardner L. and Theofanous M. Discrete and continuous treatment of local buckling in stainless steel elements. *Journal of Constructional Steel Research*, 64:1207–1216, 2008.

[51] Wilkinson T. and Hancock G. J. Tests to examine compact web slenderness of cold-formed RHS. *Journal of Structural Engineering, ASCE*, 124(10):1166–1174, 1998.

[52] Zhao X. L. and Hancock G. J. Tests to determine plate slenderness limits for cold-formed rectangular hollow sections of grade C450. *Journal of The Australian Steel Institute*, 25(4):1–16, 1991.

[53] Sedlacek G. and Feldmann M. Background document 5.09 for chapter 5 of Eurocode 3 Part 1.1: the b/t ratios controlling the applicability of analysis models in Eurocode 3 Part 1.1. Technical report, Aachen, 1995.

[54] EN 1990. *Eurocode - Basis of structural design.* European Committee for Standardization (CEN), 2002.

[55] Byfield M. P. and Nethercot D. A. Material and geometric properties of structural steel for use in design. *The Structural Engineer*, 75(21):363–367, 1997.

[56] Bock M., Mirada F. X., and Real E. Statistical evaluation of a new resistance model for cold-formed stainless steel cross-sections subjected to web crippling. *International Journal of Steel Structures*, 15(1):227–244, 2015.

[57] Davaine L. *Formulations de la résistance au lancement d'une âme métallique de pont raidie longitudinalement - Résistance dite de "Patch Loading".* L'Institut National des Sciences Appliquées de Rennes, France, 2005.
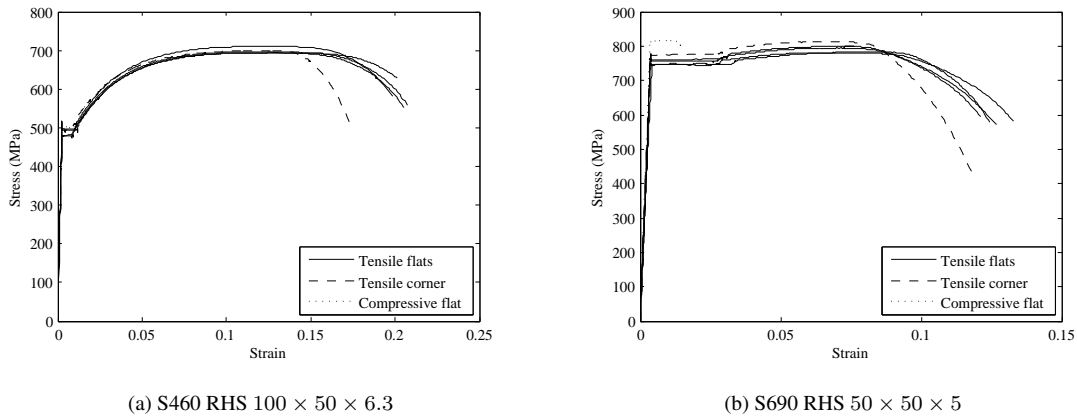
8. Figures

(a) S460 RHS $100 \times 50 \times 6.3$ (b) S690 RHS $50 \times 50 \times 5$

Figure 1: Measured stress-strain curves for tensile flat, compressive flat and tensile corner coupons extracted from a) S460 RHS $100 \times 50 \times 6.3$ and b) S690 RHS $50 \times 50 \times 5$ sections.
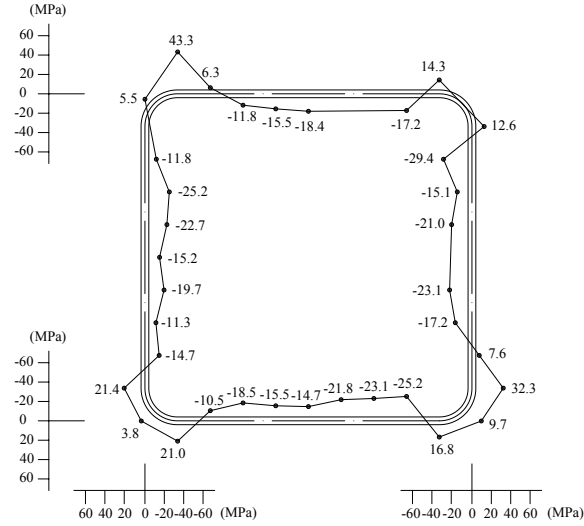
Figure 2: Measured residual stress distribution in S690 SHS $90 \times 90 \times 5.6$. Residual stresses are shown in MPa, with positive values being tensile and negative values compressive.
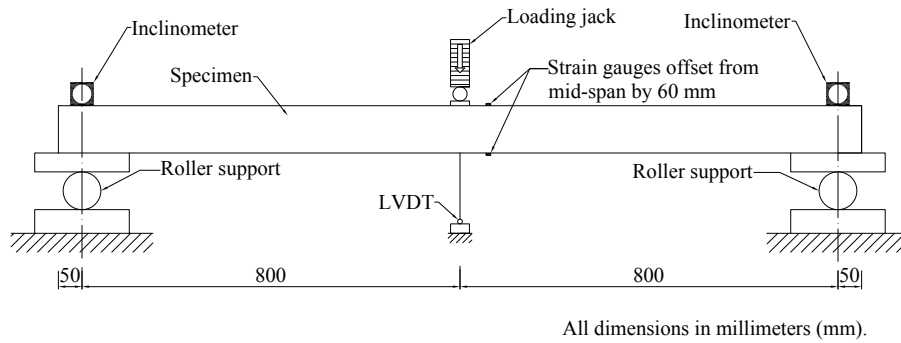

All dimensions in millimeters (mm).

Figure 3: Schematic diagram of the three-point bending test set-up.
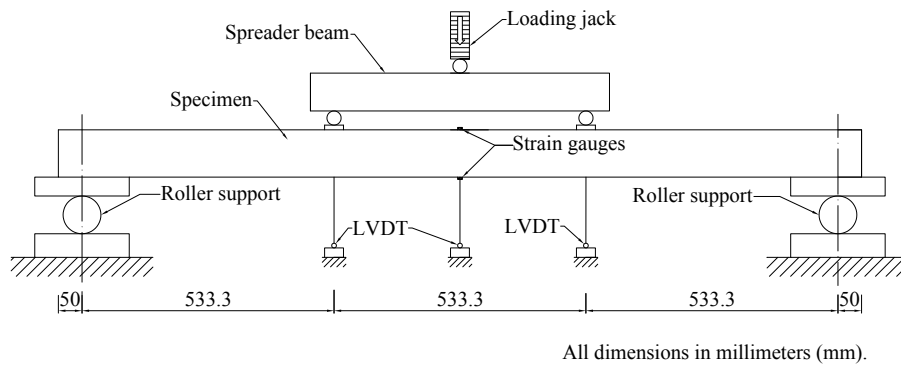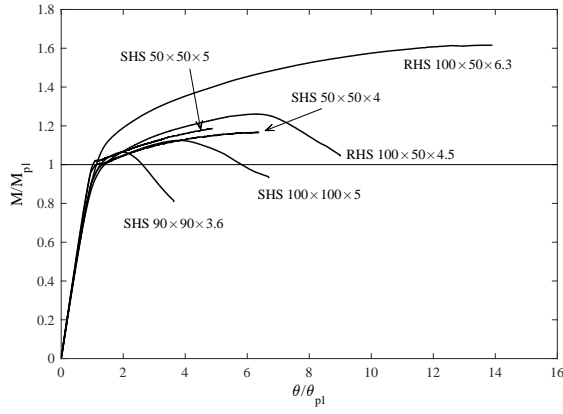

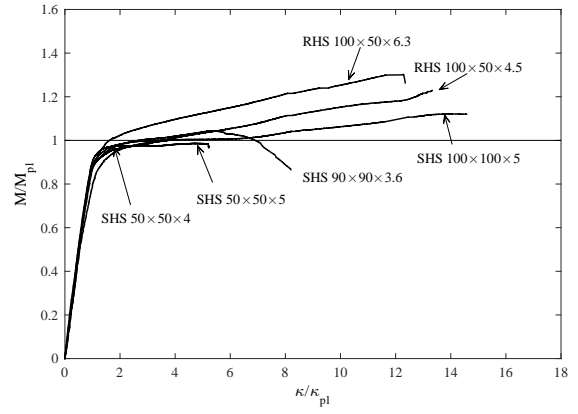All dimensions in millimeters (mm).

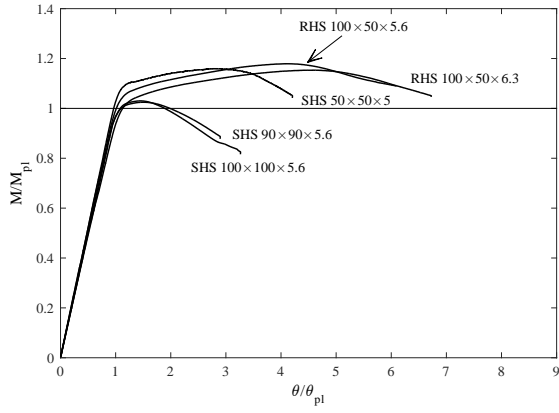Figure 4: Schematic diagram of the four-point bending test set-up.
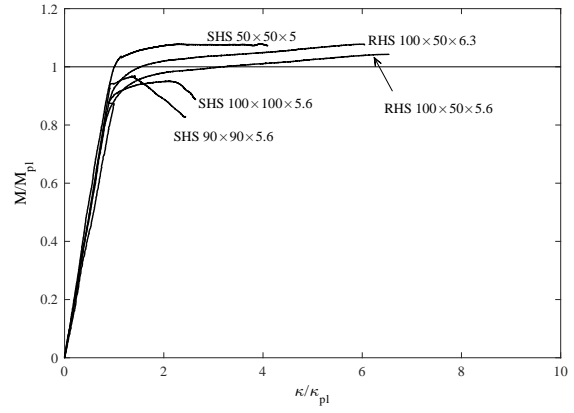
(a) Three-point bending

(b) Four-point bending

Figure 5: Normalised moment-rotation/curvature responses of S460 specimens under a) Three-point bending and b) Four-point bending.

(a) Three-point bending

(b) Four-point bending

Figure 6: Normalised moment-rotation/curvature responses of S690 specimens under a) Three-point and b) Four-point bending.
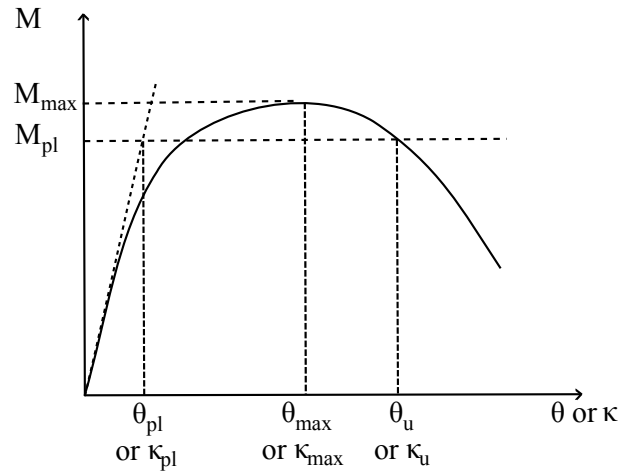
Figure 7: Definitions of parameters used for calculating the rotation capacity.

Figure 8: Typical three-point bending failure mode (S460 RHS $100 \times 50 \times 4.5$).

Figure 9: Typical four-point bending failure mode (S690 RHS $90 \times 90 \times 5.6$).
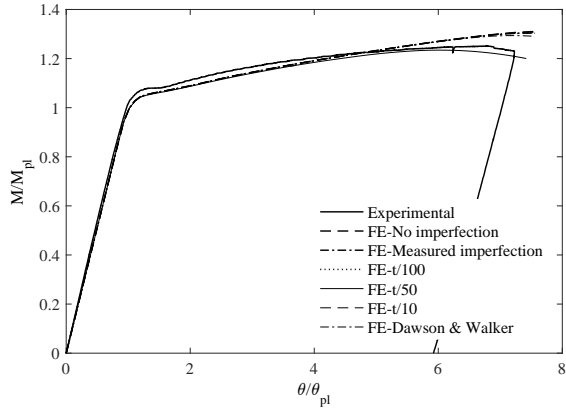
(a) S460 SHS 50×50×5
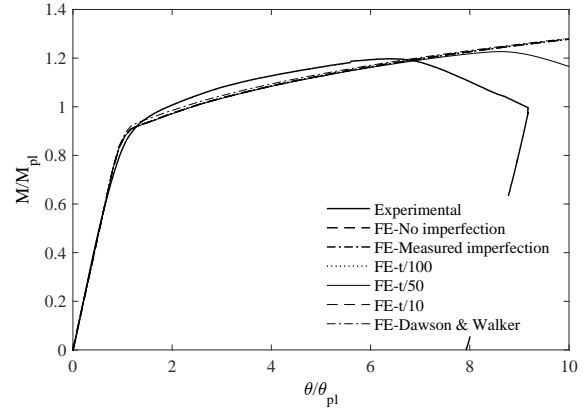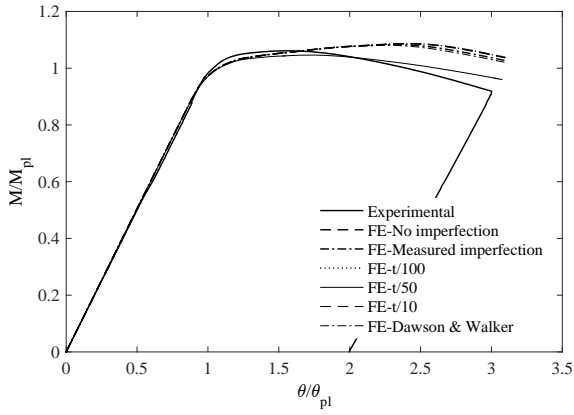
(b) S460 SHS 100×50×6.3

(c) S690 SHS 90×90×5.6
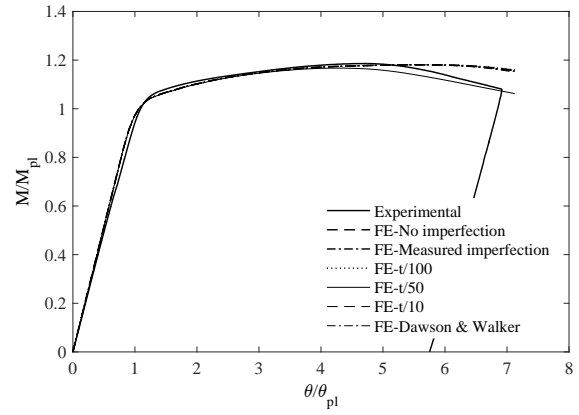
(d) S690 SHS 100×50×6.3

Figure 10: Validation of FE models with different local imperfection amplitudes for three-point bending specimens.
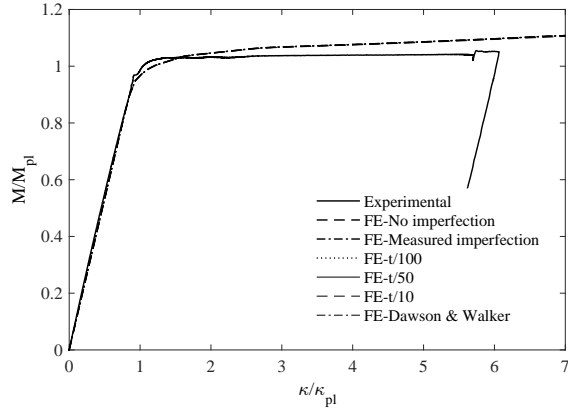
(a) S460 SHS 50×50×5
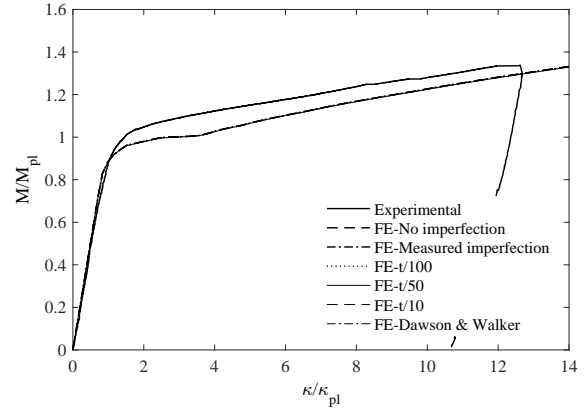
(b) S460 SHS 100×50×6.3
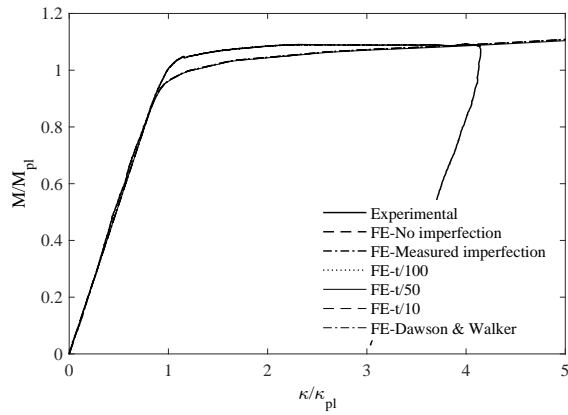
(c) S690 SHS 50×50×5
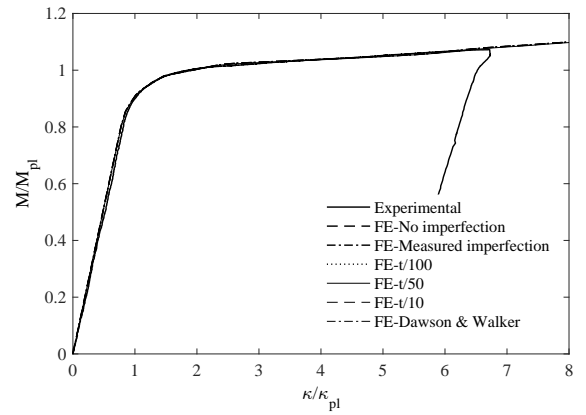
(d) S690 SHS 100×50×6.3

Figure 11: Validation of FE models with different local imperfection amplitudes for four-point bending specimens.
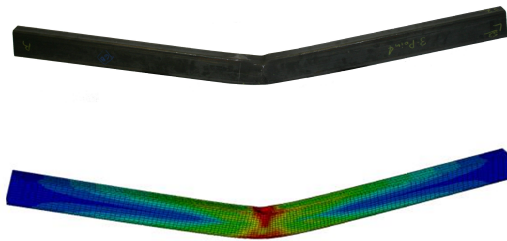
(a) S460 RHS 100×50×6.3 under three-point bending

(b) S690 SHS 50×50×5 under four-point bending

Figure 12: Typical experimental and numerical failure modes a) S460 RHS 100×50×6.3 under three-point bending; b) S690 SHS 50×50×5 under four-point bending.
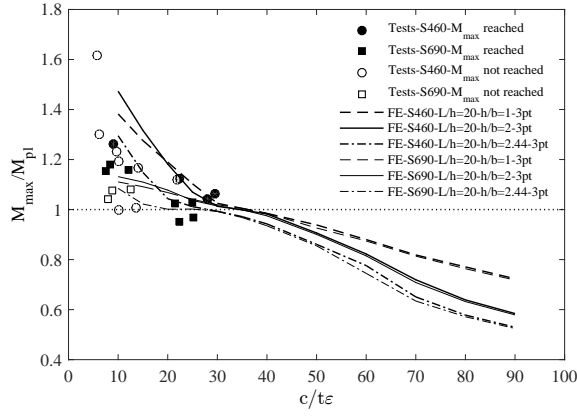
(a) Normalised moment capacity
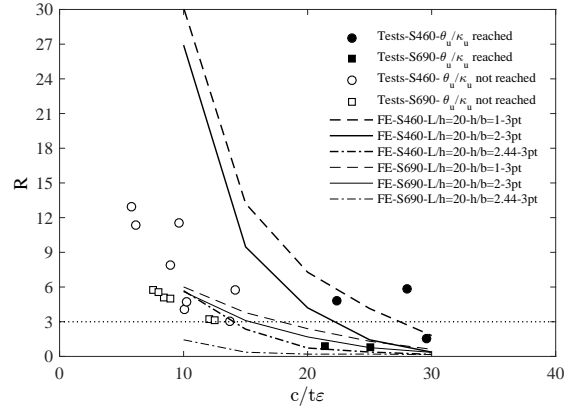
(b) Rotation capacity

Figure 13: The influence of material strain hardening and cross-section aspect ratio on a) normalised moment capacity and b) rotation capacity of SHS and RHS sections.
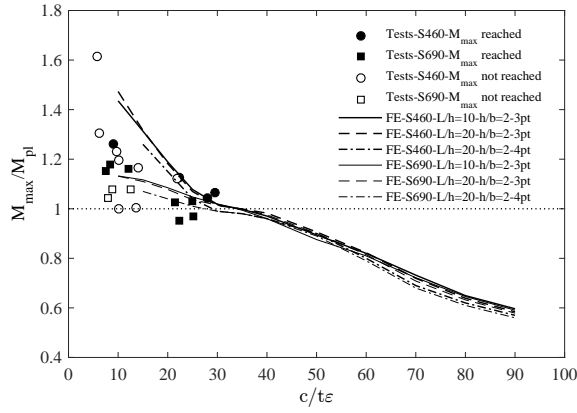
(a) Normalised moment capacity
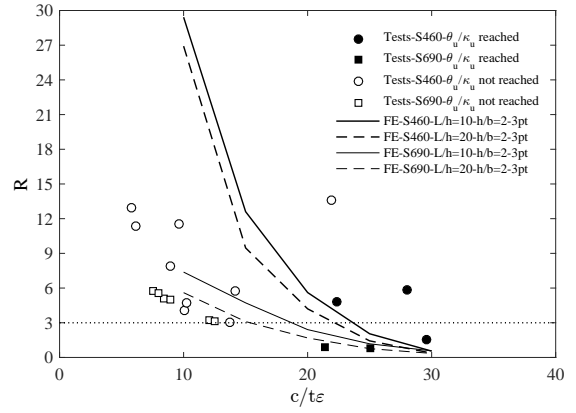
(b) Rotation capacity

Figure 14: The influence of moment gradient on a) normalised moment capacity and b) rotation capacity of RHS sections.

24
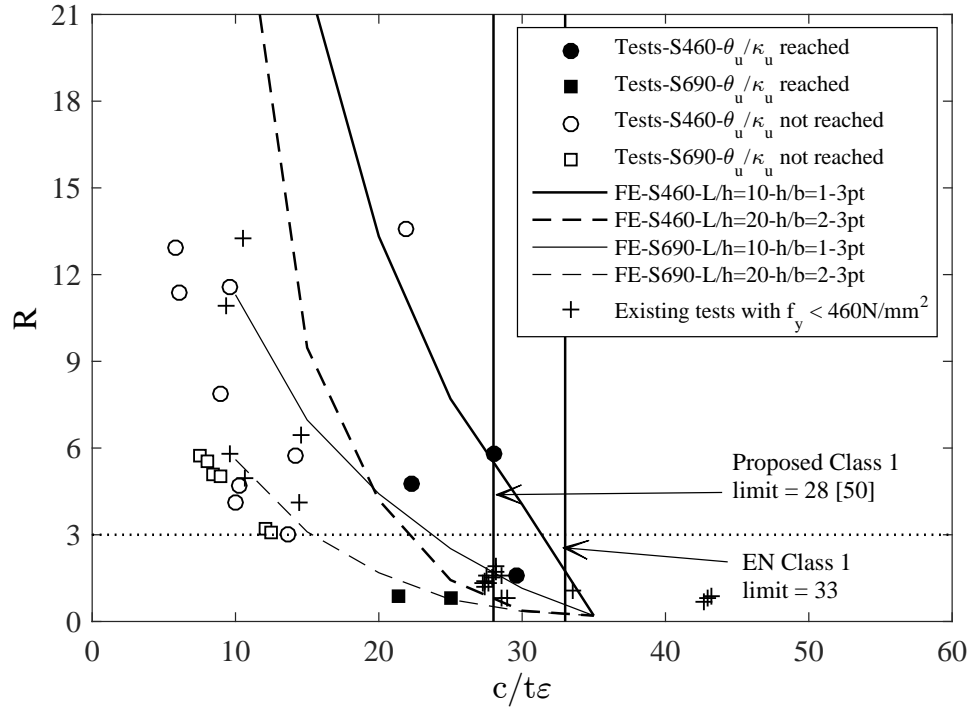
Figure 15: Assessment of Class 1 slenderness limit for internal elements in compression.
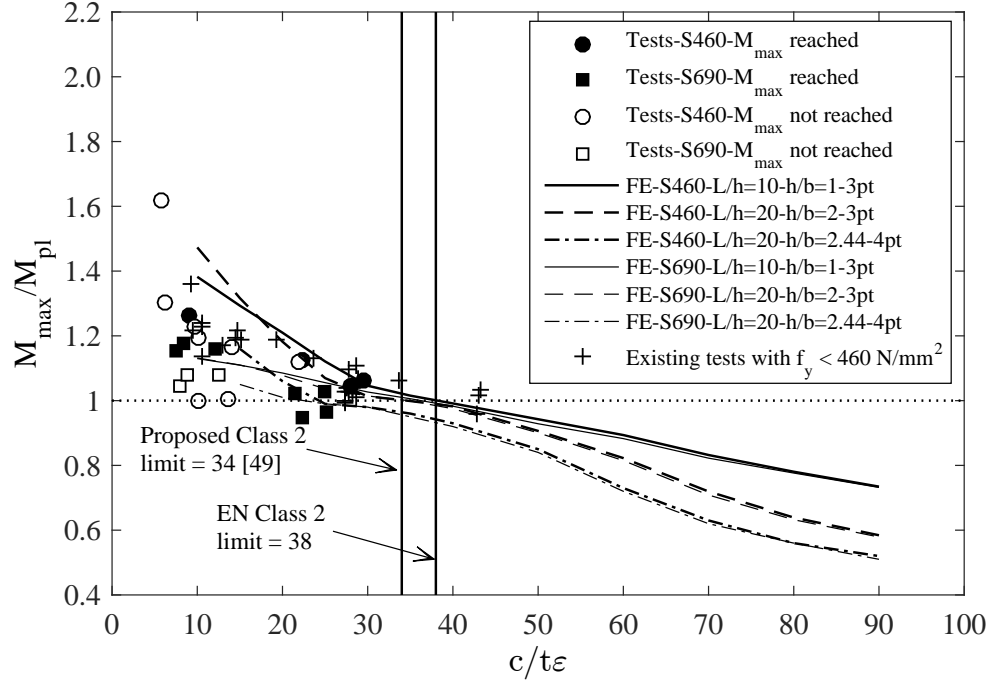
Figure 16: Assessment of Class 2 slenderness limit for internal elements in compression.
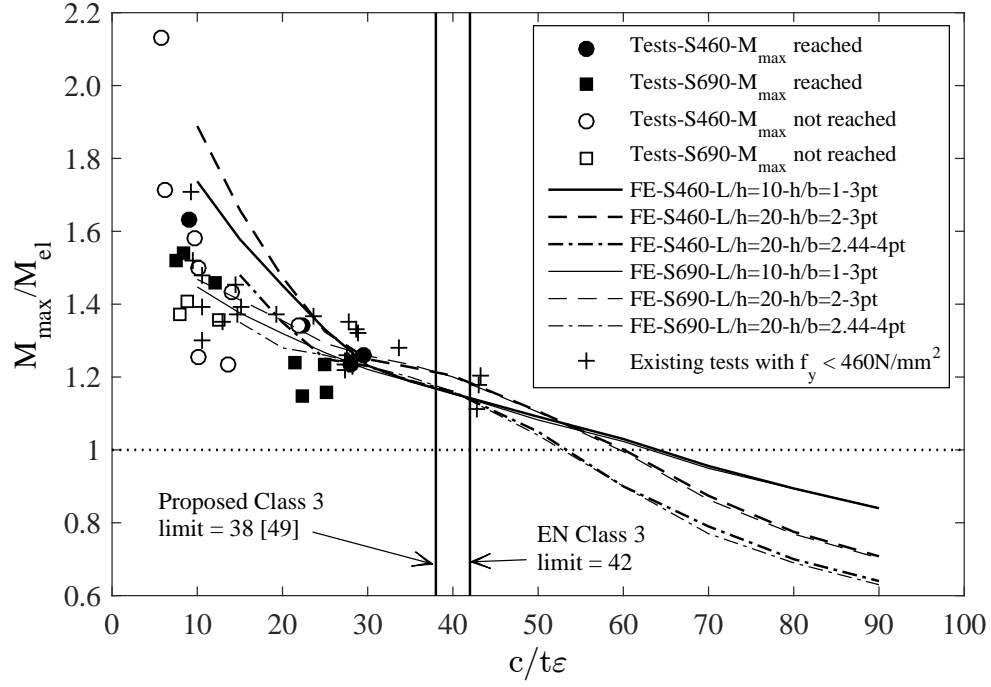
Figure 17: Assessment of Class 3 slenderness limit for internal elements in compression.
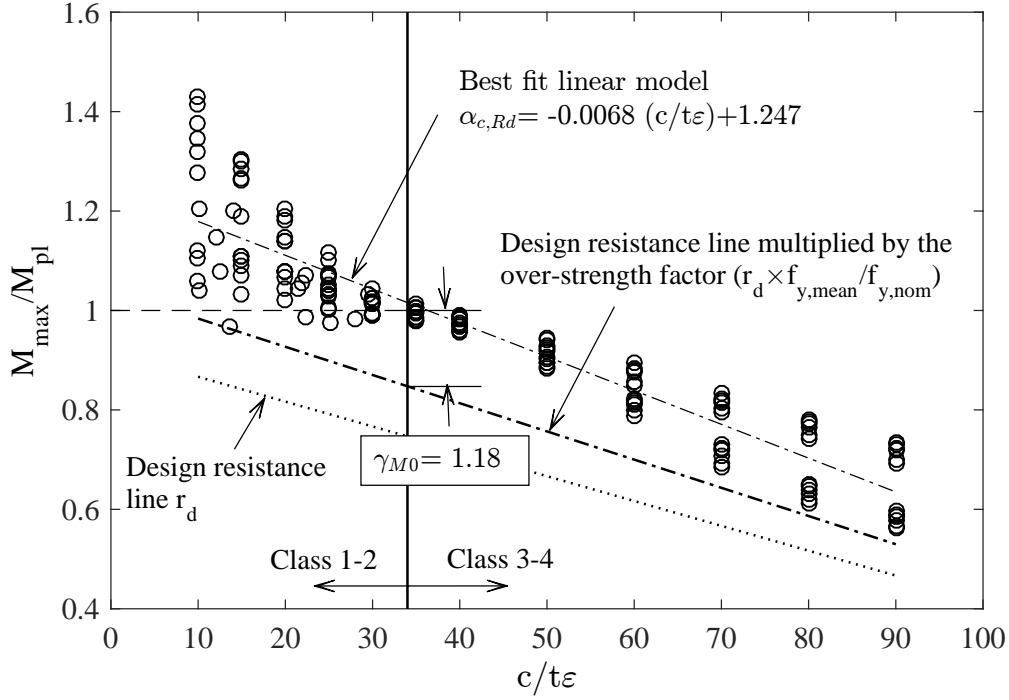
Figure 18: Determination of γ_{M0} using test and FE results for Class 2 cross-sections based on a Class 2 slenderness limit of 34.
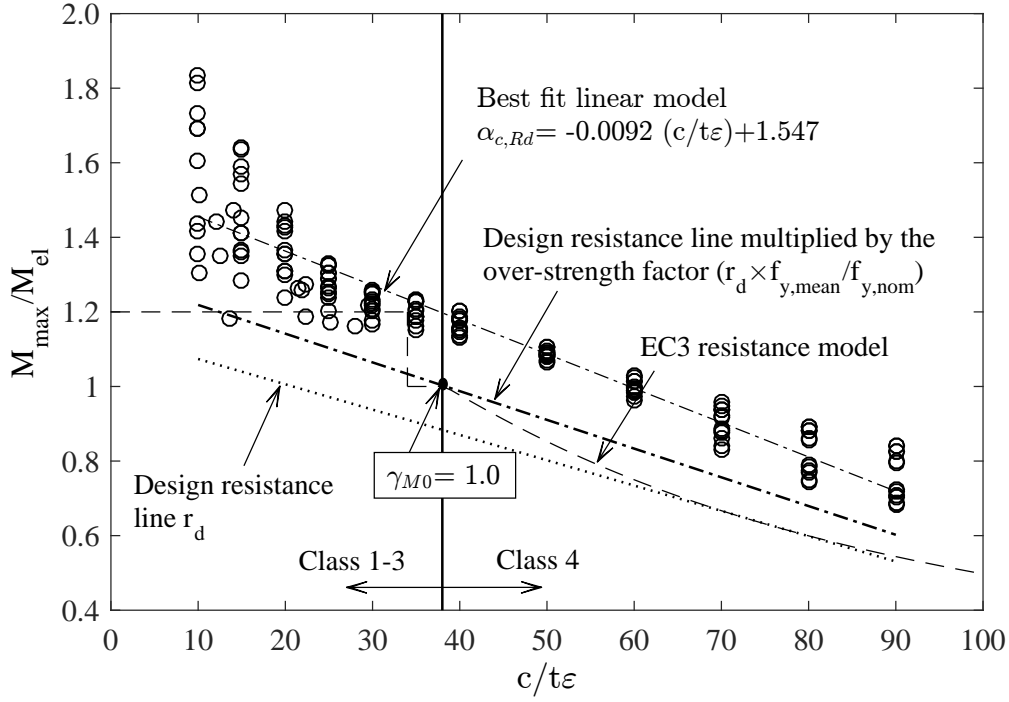
Figure 19: Determination of γ_{M0} using test and FE results for Class 3 cross-sections based on a Class 3 slenderness limit of 38.

9. Tables

Table 1: Chemical composition of tested specimens.

Grade	C	Si	Mn	P	S	Cu	Cr	Ni	Mo	V	Ti	Nb	B	Al
	(%)	(%)	(%)	(‰)	(‰)	(%)	(%)	(%)	(%)	(%)	(‰)	(‰)	(‰)	(‰)
S460 SHS 50×50×5	0.15	0.37	1.53	0.17	0.01	0.02	0.07	0.06	0.03	0.10	0.03	0.01	-	-
S460 SHS 50×50×4	0.15	0.37	1.53	0.17	0.01	0.02	0.07	0.06	0.03	0.10	0.03	0.01	-	-
S460 SHS 100×100×5	0.15	0.37	1.53	0.17	0.01	0.02	0.07	0.06	0.03	0.10	0.03	0.01	-	-
S460 SHS 90×90×3.6	0.15	0.37	1.53	0.17	0.01	0.02	0.07	0.06	0.03	0.10	0.03	0.01	-	-
S460 RHS 100×50×6.3	0.21	0.31	1.56	0.16	0.01	0.03	0.09	0.05	0.03	0.11	0.06	0.01	-	0.35
S460 RHS 100×50×4.5	0.15	0.37	1.53	0.17	0.01	0.02	0.07	0.06	0.03	0.10	0.03	0.01	-	-
S690 SHS 50×50×5	0.15	0.28	1.50	0.10	0.02	0.02	0.67	0.12	0.21	0.07	0.04	0.31	0.003	0.30
S690 SHS 100×100×5.6	0.14	0.28	1.50	0.11	0.02	0.03	0.68	0.10	0.21	0.06	0.04	0.29	0.003	0.22
S690 SHS 90×90×5.6	0.15	0.29	1.53	0.10	0.01	0.04	0.69	0.10	0.21	0.06	0.04	0.27	0.003	0.21
S690 RHS 100×50×6.3	0.15	0.28	1.50	0.10	0.02	0.02	0.67	0.12	0.21	0.07	0.04	0.31	0.003	0.30
S690 RHS 100×50×5.6	0.14	0.28	1.50	0.11	0.02	0.03	0.68	0.10	0.21	0.06	0.04	0.29	0.003	0.22

Table 2: Mechanical properties as stated in the mill certificates.

Cross-section	$f_{y,mill}$	$f_{u,mill}$	ε_f
	(MPa)	(MPa)	(%)
S460 SHS 50×50×5	473	615	26.5
S460 SHS 50×50×4	524	639	33.0
S460 SHS 100×100×5	492	619	29.0
S460 SHS 90×90×3.6	463	656	25.5
S460 RHS 100×50×6.3	495	668	23.5
S460 RHS 100×50×4.5	505	642	27.5
S690 SHS 50×50×5	797	838	22.4
S690 SHS 100×100×5.6	821	829	20.1
S690 SHS 90×90×5.6	789	825	16.6
S690 RHS 100×50×6.3	792	834	20.9
S690 RHS 100×50×5.6	778	822	19.7

Table 3: Average measured material properties from coupon tests.

Cross-section	Label	E (MPa)	f_y (MPa)	f_u (MPa)	ε_u (%)	ε_f (%)	f_u/f_y
S460 SHS 50×50×5	TF	211100	505	620	14.9	31.0	1.23
	TC	208000	481	631	12.7	26.0	1.31
	CF	219000	505	-	-	-	-
S460 SHS 50×50×4	TF	210700	523	623	15.9	28.5	1.19
	TC	202000	477	627	12.0	24.0	1.32
	CF	213000	503	-	-	-	-
S460 SHS 100×100×5	TF	211300	511	616	14.9	29.2	1.21
	TC	208000	528	636	5.8	23.0	1.20
	CF	221000	502	-	-	-	-
S460 SHS 90×90×3.6	TF	206200	500	655	14.7	27.9	1.31
	TC	189000	487	614	6.1	19.0	1.26
	CF	211000	507	-	-	-	-
S460 RHS 100×50×6.3	TF	212200	498	699	13.3	26.3	1.40
	TC	208000	505	700	17.4	26.0	1.39
	CF	210000	513	-	-	-	-
S460 RHS 100×50×4.5	TF	210200	498	645	13.9	28.3	1.30
	TC	211000	512	646	9.4	22.0	1.26
	CF	206000	499	-	-	-	-
S690 SHS 50×50×5	TF	204200	759	790	7.5	21.7	1.04
	TC	209000	782	813	6.9	18.0	1.04
	CF	220000	813	-	-	-	-
S690 SHS 100×100×5.6	TF	210300	782	798	7.0	19.2	1.02
	TC	209000	774	792	5.1	20.0	1.02
	CF	213000	793	-	-	-	-
S690 SHS 90×90×5.6	TF	205700	774	790	7.4	20.1	1.02
	TC	224000	754	784	9.0	18.0	1.04
	CF	215000	798	-	-	-	-
S690 RHS 100×50×6.3	TF	212500	799	820	7.1	19.0	1.03
	TC	213000	768	806	4.5	21.0	1.05
	CF	214000	800	-	-	-	-
S690 RHS 100×50×5.6	TF	209800	777	811	7.4	18.8	1.04
	TC	202000	771	781	4.9	19.0	1.01
	CF	222000	811	-	-	-	-

Table 4: Averaged measured dimensions for three-point and four-point bending specimens.

Specimen	L	h	b	t	r_i	ω_0
	(mm)	(mm)	(mm)	(mm)	(mm)	(mm)
S460 SHS 50×50×5	1700	50.41	50.36	4.92	3.25	0.054
S460 SHS 50×50×4	1700	50.37	50.47	3.89	3.19	0.043
S460 SHS 100×100×5	1700	99.76	99.67	5.29	4.88	0.077
S460 SHS 90×90×3.6	1700	89.79	89.64	3.71	4.50	0.083
S460 RHS 100×50×6.3	1700	99.82	49.83	6.40	5.44	0.049
S460 RHS 100×50×4.5	1700	99.59	49.94	4.64	5.50	0.070
S690 SHS 50×50×5	1700	50.44	50.53	4.94	3.46	0.076
S690 SHS 100×100×5.6	1700	100.53	100.47	5.66	5.59	0.081
S690 SHS 90×90×5.6	1700	90.48	90.46	5.74	4.92	0.089
S690 RHS 100×50×6.3	1700	100.27	49.92	6.46	4.88	0.106
S690 RHS 100×50×5.6	1700	100.51	49.89	5.69	5.75	0.156

Table 5: Summary of results from three-point bending tests.

Specimen	$c/t\varepsilon$	M_{max}	θ_{max}	θ_u	M_{el}	M_{pl}	M_{max}/M_{el}	M_{max}/M_{pl}	R
		(kNm)	(rad)	(rad)	(kNm)	(kNm)			
S460 SHS 50×50×5	10.06	8.67*	0.24*	0.24**	5.78	7.26	1.50*	1.19*	> 4.09**
S460 SHS 50×50×4	14.16	7.17*	0.33*	0.33**	5.01	6.14	1.43*	1.17*	> 5.74**
S460 SHS 100×100×5	22.32	38.88	0.09	0.13	28.94	34.57	1.34	1.12	4.79
S460 SHS 90×90×3.6	29.59	20.73	0.07	0.07	16.51	19.47	1.26	1.06	1.59
S460 RHS 100×50×6.3	5.76	39.26*	0.35*	0.35**	18.43	24.30	2.13*	1.62*	> 12.91**
S460 RHS 100×50×4.5	8.95	23.68	0.15	0.22**	14.57	18.78	1.63	1.26	> 7.89**
S690 SHS 50×50×5	12.04	12.56	0.20	0.31**	8.61	10.83	1.46	1.16	> 3.21**
S690 SHS 100×100×5.6	25.04	58.25	0.05	0.07	47.11	56.55	1.24	1.03	0.83
S690 SHS 90×90×5.6	21.42	46.59	0.06	0.08	37.55	45.46	1.24	1.02	0.89
S690 RHS 100×50×6.3	7.54	46.44	0.18	0.27**	30.57	40.26	1.52	1.15	> 5.73**
S690 RHS 100×50×5.6	8.38	41.69	0.16	0.24**	27.03	35.36	1.54	1.18	> 5.10**

* Test discontinued before M_{max} or θ_{max} were reached.

** Test discontinued before moment fell below M_{pl} on descending branch.

Table 6: Summary of results from four-point bending tests.

Specimen	$c/t\varepsilon$	M_{max} (kNm)	$\kappa_{max}(\times 10^{-4})$ (mm^{-1})	$\kappa_{u}(\times 10^{-4})$ (mm^{-1})	M_{el} (kNm)	M_{pl} (kNm)	M_{max}/M_{el}	M_{max}/M_{pl}	R
S460 SHS 50×50×5	10.21	7.03*	6.83*	6.83**	5.61	7.04	1.25*	1.00*	>4.72**
S460 SHS 50×50×4	13.70	6.25*	4.88*	4.88**	5.06	6.22	1.24*	1.01*	>3.03**
S460 SHS 100×100×5	21.92	38.61*	8.06*	8.46**	28.79	34.42	1.34*	1.12*	>13.59**
S460 SHS 90×90×3.6	28.01	20.81	3.34	4.35	16.87	19.94	1.23	1.04	5.83
S460 RHS 100×50×6.3	6.41	32.46*	7.60*	7.64**	18.94	24.91	1.71*	1.30*	>11.35**
S460 RHS 100×50×4.5	9.67	23.28*	7.67*	7.67**	14.74	18.93	1.58*	1.23*	>11.55**
S690 SHS 50×50×5	12.51	11.59*	7.27*	7.55**	8.55	10.74	1.36*	1.08*	>3.10**
S690 SHS 100×100×5.6	25.20	54.91	1.21	1.21	47.32	56.78	1.16	0.97	-
S690 SHS 90×90×5.6	22.31	42.88	2.08	2.08	37.37	45.14	1.15	0.95	-
S690 RHS 100×50×6.3	8.00	42.25*	6.42*	6.45**	30.83	40.51	1.37*	1.04*	>5.54**
S690 RHS 100×50×5.6	8.91	37.87*	5.79*	5.81**	26.93	35.13	1.41*	1.08*	>5.05**

* Test discontinued before M_{max} or θ_{max} were reached.

** Test discontinued before moment fell below M_{pl} on descending branch.

Table 7: Comparison of FE and test data for three-point bending tests.

Specimen	Imperfection amplitude											
	0		ω_0		t/100		t/50		t/10		Dawson&Walker	
	$\frac{M_{max,FE}}{M_{max,exp}}$	$\frac{\theta_{max,FE}}{\theta_{max,exp}}$	$\frac{M_{max,FE}}{M_{max,exp}}$	$\frac{\theta_{max,FE}}{\theta_{max,exp}}$	$\frac{M_{max,FE}}{M_{max,exp}}$	$\frac{\theta_{max,FE}}{\theta_{max,exp}}$	$\frac{M_{max,FE}}{M_{max,exp}}$	$\frac{\theta_{max,FE}}{\theta_{max,exp}}$	$\frac{M_{max,FE}}{M_{max,exp}}$	$\frac{\theta_{max,FE}}{\theta_{max,exp}}$	$\frac{M_{max,FE}}{M_{max,exp}}$	$\frac{\theta_{max,FE}}{\theta_{max,exp}}$
S460 SHS 50×50×5	1.01	1.01	1.01	1.01	1.01	1.01	1.01	1.01	1.01	1.01	1.01	1.01
S460 SHS 50×50×4	1.05	1.09	1.04	1.09	1.04	1.09	1.03	1.05	0.99	0.89	1.04	1.09
S460 SHS 100×100×5	0.98	1.15	0.95	0.96	0.96	1.01	0.95	0.94	0.9	0.88	0.96	1.01
S460 SHS 90×90×3.6	0.98	1.05	0.96	0.96	0.98	1.05	0.97	0.96	0.92	1.14	0.97	0.98
S460 RHS 100×50×6.3	1.01	1.01	1.01	1.01	1.01	1.01	1.00	1.02	0.98	0.96	1.01	1.01
S460 RHS 100×50×4.5	1.06	1.53	1.06	1.53	1.06	1.53	1.06	1.51	1.02	1.03	1.06	1.52
S690 SHS 50×50×5	0.99	1.17	0.99	1.15	0.99	1.17	0.99	1.14	0.97	0.97	0.99	1.17
S690 SHS 100×100×5.6	1.01	1.39	1.00	1.25	1.00	1.28	1.00	1.27	0.97	0.91	1.00	1.25
S690 SHS 90×90×5.6	1.02	1.55	1.02	1.48	1.02	1.55	1.02	1.49	0.99	1.13	1.02	1.53
S690 RHS 100×50×6.3	1.00	1.18	1.00	1.18	1.00	1.20	1.00	1.18	0.98	0.91	1.00	1.19
S690 RHS 100×50×5.6	0.98	1.23	0.98	1.11	0.98	1.21	0.98	1.15	0.96	0.91	0.98	1.21
Mean	1.01	1.21	1.00	1.16	1.01	1.19	1.01	1.16	0.97	0.98	1.01	1.18
COV	0.03	0.15	0.03	0.16	0.03	0.16	0.03	0.16	0.04	0.09	0.03	0.16

Table 8: Comparison of FE and test data for four-point bending tests.

Specimen	Imperfection amplitude											
	0		ω_0		t/100		t/50		t/10		Dawson&Walker	
	$\frac{M_{max,FE}}{M_{max,exp}}$	$\frac{\kappa_{max,FE}}{\kappa_{max,exp}}$	$\frac{M_{max,FE}}{M_{max,exp}}$	$\frac{\kappa_{max,FE}}{\kappa_{max,exp}}$	$\frac{M_{max,FE}}{M_{max,exp}}$	$\frac{\kappa_{max,FE}}{\kappa_{max,exp}}$	$\frac{M_{max,FE}}{M_{max,exp}}$	$\frac{\kappa_{max,FE}}{\kappa_{max,exp}}$	$\frac{M_{max,FE}}{M_{max,exp}}$	$\frac{\kappa_{max,FE}}{\kappa_{max,exp}}$	$\frac{M_{max,FE}}{M_{max,exp}}$	$\frac{\kappa_{max,FE}}{\kappa_{max,exp}}$
S460 SHS 50×50×5	1.04	1.00	1.04	1.00	1.04	1.00	1.04	1.00	1.03	1.00	1.04	1.00
S460 SHS 50×50×4	0.96	1.02	0.96	1.02	0.95	0.86	0.95	0.86	0.95	0.87	0.95	0.88
S460 SHS 100×100×5	0.96	1.03	0.95	1.05	0.96	1.04	0.94	1.02	0.86	0.86	0.95	1.05
S460 SHS 90×90×3.6	1.01	1.51	0.93	0.99	0.96	1.20	0.94	1.03	0.92	0.91	0.95	1.08
S460 RHS 100×50×6.3	0.97	1.00	0.97	1.00	0.97	1.00	0.97	1.00	0.97	0.99	0.97	1.00
S460 RHS 100×50×4.5	0.96	0.99	0.96	0.99	0.96	0.99	0.96	0.99	0.95	0.99	0.96	0.99
S690 SHS 50×50×5	1.00	1.03	1.00	1.03	1.00	1.03	1.00	1.03	1.00	1.03	1.00	1.03
S690 SHS 100×100×5.6	1.01	1.03	1.01	1.03	1.01	1.03	1.01	1.03	1.00	1.00	1.01	1.03
S690 SHS 90×90×5.6	1.04	1.67	1.04	1.67	1.04	1.67	1.04	1.67	1.03	1.64	1.04	1.67
S690 RHS 100×50×6.3	1.01	1.01	1.01	1.01	1.01	1.01	1.01	1.01	1.01	1.02	1.01	1.01
S690 RHS 100×50×5.6	0.98	1.01	0.98	1.01	0.98	1.01	0.98	1.01	0.98	1.01	0.98	1.01
Mean	0.99	1.12	0.99	1.07	0.99	1.08	0.99	1.07	0.97	1.03	0.99	1.07
COV	0.03	0.20	0.03	0.18	0.03	0.19	0.04	0.19	0.05	0.20	0.03	0.18

Table 9: Summary of the reliability analysis results

Classification limit		n	$k_{d,n}$	b	V_δ	V_r	γ_{M0}
Class 2 limit	EN 1993-1-1 (38)	95	3.196	1.002	0.064	0.094	1.20
	Proposed (34)	83	3.212	1.002	0.069	0.097	1.18
Class 3 limit	EN 1993-1-1 (42)	95	3.196	1.021	0.072	0.099	1.02
	Proposed (38)	83	3.212	1.023	0.077	0.102	1.00